Journal of Sound and Vibration 326 (2009) 557–573

Contents lists available at ScienceDirect

Journal of Sound and Vibration

journal homepage: www.elsevier.com/locate/jsvi

# Structural model updating using frequency response function and quasi-linear sensitivity equation

A. Esfandiari [a,b], F. Bakhtiari-Nejad [a], A. Rahai [a], M. Sanayei [b,*]

[a] Amirkabir University of Technology, Tehran, Iran
[b] Tufts University, MA, USA

ARTICLE INFO

*Article history:*
Received 18 January 2009
Received in revised form
1 July 2009
Accepted 2 July 2009
Handling Editor: C.L. Morfey

ABSTRACT

A method is presented for structural mass and stiffness estimation including damping effects and using vibration data. It uses the frequency response function (FRF) and natural frequencies data for finite element model updating. The FRF data are compiled using the measured displacement, velocity or acceleration of the damaged structure. A least-square algorithm method with appropriate normalization is used for solving the over-determined system of equations with noise-polluted data. Sensitivity equation normalization and proper selection of measured frequency points improved the accuracy and convergence in finite element model updating. Using simulated measurements shows that this method can detect, locate and quantify the severity of damage within structures.



## 1. Introduction

Early structural damage detection is desirable to prevent structural failure and human loss of life. Non-destructive testing (NDT) methods can complement visual inspections as an objective method leading to quantifiable results. Current NDT techniques such as ultrasound, X-ray, dye penetrates, magnetic particle, and acoustic emission are often limited to observation in a limited area and rely on a presumption of the likely area of damage. Structural damage detection using non-destructive vibration test data has received considerable attention since early in the decade. The basic principle is that occurrence of damage will change the static and dynamic characteristics such as displacement, strain, natural frequencies, damping loss factors, mode shapes and frequency response function (FRF). The ability to detect and quantify these changes demonstrate that it is feasible to use FRFs for damage diagnosis and health monitoring of aerospace, mechanical, and civil engineering structural systems.

Existing structural parameter identification methods can be classified into several groups depending on the type of acquired data used to detect, locate, and/or quantify structural damage. They include changes in modal data [1–5], frequency response functions [6,7], strain energy [8], transfer function parameters [9], flexibility matrix [10], residual forces [11], mechanical impedances [12] and so forth. Most of the literature on structural damage detection relies on using modal analysis data that are extracted from FRF data, the most compact form of vibration data. An extensive review on the subject can be found in [13,14]. Such methods are based on algorithms involving extensive numerical computing processes, matrix inversion, and curve fitting techniques. As discussed by Banks et al. [15], the structural damage detection methods based on modal data have some shortcomings. Because the modal data are indirectly measured test data, they could be

* Corresponding author. Tel.: +1 617 627 3211.
*E-mail address:* masoud.sanayei@tufts.edu (M. Sanayei).

0022-460X/$ - see front matter © 2009 Elsevier Ltd. All rights reserved.
doi:10.1016/j.jsv.2009.07.001

contaminated by measurement errors and modal extraction errors. In addition, complete modal data cannot practically be obtained in most cases because they often require a large number of sensors.

In this paper, the authors address the challenges in using measured FRF data and present methods for successful use of such data for finite element model updating. Vibration-based damage detection using measured FRF has been studied by a number of researchers [16–21]. There are several advantages in using direct FRF measurements. FRF data can be extracted without further numerical processing and hence will not be contaminated by modal extraction errors and loss of information due to the curve fitting. Because of this, it is more reliable and practical to use directly-measured FRF data for finite element model updating for structural damage detection, particularly for structures with closely spaced modes. FRF-based damage detection methods can provide abundant information at measured degrees of freedom and at a great number of desired frequencies [18], as opposed to modal data, which are extracted from a very limited number of FRF data at resonance frequencies. Also, FRF data in the vicinity of resonant frequencies is not necessary to provide the most reliable damage detection [22]. The proper selection of frequency ranges must be addressed by choosing 'regions' of FRF that are not adversely corrupted by noise. If improper frequency points are adopted, the measurement error may seriously affect the results. Due to the aforementioned advantages of FRF data over the modal data, it seems very promising to use the measured FRF data for identifying structural damage [23–25].

Furukawa et al. [26] combine the deterministic damage identification technique with hypothesis testing based on the bootstrap method, using harmonic excitation force data. They investigate the uncertainty effect of measurement noise and modeling errors in the baseline model. Lee and Shin [27,28] developed a structural damage identification method for beam and plate structure using FRF data. They applied a concept of reduced-domain method to iteratively search out and remove damage-free zones from the original domain of the problem. They extended their method to orthotropic plates [29].

Ni et al. [30] investigate the efficiency of the principle component analysis (PCA) concept to identify the seismic damage of a 1:20 scale model of a 38-storey reinforced concrete building using measured FRFs and neural networks on a shaking table. It is shown that the identification results by means of the FRF projections on a few principal components are much better than those obtained directly using the measured FRF data. Hwang and Kim [31] used FRF data to find the location and severity of damage in structures by considering only a vector subset of the full set of FRFs. Zimmerman et al. [32] extend previous developments in minimum rank perturbation theory (MRPT) for damage detection through the FRF concept. The algorithm sensitivity to noise is investigated using different experimental and numerical test data sets for two setups: the NASA 8-bay truss and the I-40 bridge over the Rio Grande. The FRF-based results are shown to be insensitive to noise if proper frequency lines are used and provide a damage assessment similar to that obtained using identified modal parameters, but at a substantially reduced level of effort.

Araujo dos Santos et al. [33] propose a damage identification method based on FRF sensitivities. They indicate that better identification results are obtained in lower frequency ranges and excitation points where there are no nodes. It was found that the number of required mode shapes to constructed FRF matrices should be at least three times the number of contained natural frequencies and mode shapes in the desired range of frequency. It is demonstrated that for small amounts of damage the measurement errors are the main influence in the identification quality, whereas for larger amounts of damage the incompleteness of measurements becomes the most important factor. A procedure for weighting and deletion of equations is used to improve the identification results.

In this work a FRF-based finite element model updating algorithm is presented using harmonic forced vibration FRF of the damaged structure. Changes in the FRF of structures due to damage are correlated to changes of stiffness, mass and damping properties through damage sensitivity equations, which have been derived using the FRF of intact structures and measured natural frequencies. Examples of the unknown structural stiffness and mass parameters that will be updated in this process are axial rigidity (EA), bending rigidity (EI), torsional rigidity (GJ), and mass per unit length ($\bar{m}$). The impedance matrix of the damaged structures is approximated by using the measured natural frequencies of the damaged structure and normalized mode shapes of the undamaged (or intact) structure. Damage sensitivity equations are solved by the least square method through proper normalization procedure. The effect of excitation frequency and weighting methods on results has been addressed. A truss model example is used to show successful structural parameter estimation for finite element model updating and damage assessment using noisy FRF data.

## 2. Theoretical development

A general mathematical derivation of equation of motion of an $n$ degree of freedom system is given as

$$\mathbf{M}\ddot{\mathbf{x}} + \mathbf{C}\dot{\mathbf{x}} + \mathbf{K}\mathbf{x} = \mathbf{f}(t) \tag{1}$$

where $\mathbf{M}$, $\mathbf{C}$ and $\mathbf{K}$ are $n \times n$ mass, damping and stiffness matrices, respectively. $\mathbf{f}(t)$ is an $n \times 1$ vector of applied force and $\mathbf{x}$, $\dot{\mathbf{x}}$ and $\ddot{\mathbf{x}}$ are $n \times 1$ vectors of the structural displacement, velocity and acceleration. Assuming a harmonic input, the applied force and displacement response vectors can be expressed as

$$\mathbf{f}(t) = \mathbf{F}(\omega)\mathrm{e}^{\mathrm{j}\omega t} \quad \text{and} \quad \mathbf{f}(t) = \mathbf{X}(\omega)\mathrm{e}^{\mathrm{j}\omega t} \tag{2}$$

where $\omega$ is the frequency of the excitation load and $\mathrm{j} = \sqrt{-1}$. Substituting Eq. (2) into Eq. (1) yields

$$(-\omega^2\mathbf{M} + \mathrm{j}\omega\mathbf{C} + \mathbf{K})\mathbf{X}(\omega)\mathrm{e}^{\mathrm{j}\omega t} = \mathbf{F}(\omega)\mathrm{e}^{\mathrm{j}\omega t} \tag{3}$$

Defining

$$\mathbf{B}(\omega) = (-\omega^2\mathbf{M} + \mathrm{j}\omega\mathbf{C} + \mathbf{K}) \tag{4}$$

Eq. (3) can be written as

$$\mathbf{B}(\omega)\mathbf{X}(\omega) = \mathbf{F}(\omega) \tag{5}$$

where $\mathbf{B}(\omega)$ is an $n \times n$ matrix referred to as the system impedance matrix or, for simplicity, the system matrix. Then the transfer functions matrix $\mathbf{H}(\omega)$ is an $n \times n$ matrix that can be defined in terms of the system characteristics such as mass, stiffness, and damping as

$$\mathbf{H}(\omega) = \mathbf{B}(\omega)^{-1} = (-\omega^2\mathbf{M} + \mathrm{j}\omega\mathbf{C} + \mathbf{K})^{-1} \tag{6}$$

and structural response can be calculated in frequency domain as

$$\mathbf{X}(\omega) = \mathbf{H}(\omega)\mathbf{F}(\omega) \tag{7}$$

It is assumed that the damage causes the changes in the stiffness, mass and damping matrices by amount of $\delta\mathbf{K}$, $\delta\mathbf{M}$ and $\delta\mathbf{C}$ respectively. These changes are proportional to system parameters and obey the general connectivity of the structure. The forced vibration Eq. (7) can be rewritten as

$$(-\omega^2(\mathbf{M} + \delta\mathbf{M}) + \mathrm{j}\omega(\mathbf{C} + \delta\mathbf{C}) + \mathbf{K} + \delta\mathbf{K})(\mathbf{X}(\omega) + \delta\mathbf{X}(\omega)) = \mathbf{F}(\omega) \tag{8}$$

An analytical representation of the change in the response is determined by expanding (8) and subtracting (7), yielding

$$\delta\mathbf{X}(\omega) = -\mathbf{H}_d(\omega)(\delta\mathbf{K} + \mathrm{j}\omega\delta\mathbf{C} - \omega^2\delta\mathbf{M})\mathbf{X}(\omega) \tag{9}$$

where $\delta\mathbf{X}(\omega)$ is the change in dynamic response at each frequency due to damage and the FRF of the damaged structure is

$$\mathbf{H}_d(\omega) = (-\omega^2(\mathbf{M} + \delta\mathbf{M}) + \mathrm{j}\omega(\mathbf{C} + \delta\mathbf{C}) + \mathbf{K} + \delta\mathbf{K})^{-1} \tag{10}$$

Eq. (9) expresses the dependence of the response of the structure on the changes of the stiffness, mass and damping matrices.

The complete transfer function of the damaged structure $\mathbf{H}_d(\omega)$ is required to construct Eq. (9), which necessitates measurements at all DOFs. This is quite impractical. In an iterative procedure one may approximate it either by the transfer function of the intact structure, or by evaluating it by Taylor series expansion using the derivative of $\mathbf{H}(\omega)$, which will increase the order of equations. Another issue is that the derivative of $\mathbf{H}(\omega)$ is a highly discontinuous and non-monotonous function for lightly damped structures.

The transfer function matrix $\mathbf{H}(\omega)$ can be decomposed in modal coordinates using mode shapes and natural frequencies as

$$\mathbf{H}_d(\omega) = \sum_{i=1}^{m} \frac{\phi_i\phi_i^T}{\Omega_i^2 - \omega^2 + 2\mathrm{j}\xi_i\Omega_i\omega} \tag{11}$$

where $\phi_i$ is the $i$th mode shape of the structure, $\Omega_i$ represents the $i$th natural frequency, $\omega$ is the excitation frequency, and $\xi_i$ is the modal damping loss factor of the $i$th mode shape. As an approximation, one may use a truncated form of (11) to compute transfer function in the decomposed form using a subset of modal characteristics. The number of required mode shapes is dependent on the magnitude of the excitation frequency in comparison to the natural frequencies. As stated by Araujo dos Santos et al. [38], for a well-defined approximation of $\mathbf{H}(\omega)$ the number of the measured natural frequencies must be large enough in comparison to the maximum applied excitation frequency. They state that the frequency of the last considered mode of vibration in the truncated form must be at least three times that of the excitation frequency.

Since it is impractical to measure all natural frequencies and identify mode shapes at all DOFs for the damaged structures, in order to obtain a practical representation of the $\mathbf{H}_d(\omega)$ it is approximated using the analytical mode shapes of the intact structure $\phi$, the measured natural frequencies of the damaged structure $\Omega_{id}$ and measured damping loss factor $\xi_{id}$ as

$$\mathbf{H}_d(\omega) \cong \sum_{i=1}^{m} \frac{\phi_i\phi_i^T}{\Omega_{id}^2 - \omega^2 + 2\mathrm{j}\xi_{id}\Omega_{id}\omega} + \sum_{i=m+1}^{n} \frac{\phi_i\phi_i^T}{\Omega_i^2 - \omega^2 + 2\mathrm{j}\xi_i\Omega_i\omega} \tag{12}$$

where $m$ is the number of the measured natural frequencies and $n$ is the number of DOFs. This approximation in (12) is realistic because it is possible to measure natural frequencies with high accuracy. The second term is related to the unmeasured part of $\mathbf{H}_d(\omega)$, and is used to alleviate incomplete measurements effects. Numerical simulation shows that this part increases the accuracy of (12) and convergence rate. Eq. (12) improves its accuracy by updating $\phi_i$ and $\Omega_i$ as the optimization process updates the parameters of the structure. The advantage of using an approximate computation of the transfer function is that the derivative of $\mathbf{H}(\omega)$ is avoided. It will be shown numerically that (12) is a good approximation of $\mathbf{H}_d(\omega)$. Also, $\mathbf{B}(\omega)$ in (4) is a linear explicit function of the parameters [34], so its derivative $(-\omega^2\delta\mathbf{M}+\mathrm{j}\omega\delta\mathbf{C}+\delta\mathbf{K})$, shows a smooth behavior and its computation is numerically stable.

Using sensitivity Eq. (9) one can simultaneously estimate stiffness, mass and damping properties of the damaged structure. Generally, energy dissipation and damping are not only related to the material property of individual elements, but are also caused by structural connections, joints and non-structural members, which are not modeled in most of finite element modeling. Depending on the case study and structural behavior, one may prefer to use measured data to model damping by modal or structural damping model. Since in this method natural frequencies and damping loss factors are measured, it is possible to model damping by the desired model and use it in (9). Using measured modal damping factors will reduce the number of unknowns and the number of required measurements for model updating. Also, damping of the structure is far more significant at resonance frequencies as it dominates the amplitude of FRF. The damping influence on the response rapidly decreases by moving away from the resonance frequencies.

The global stiffness matrix $\mathbf{K}$ and mass matrix $\mathbf{M}$ will be updated using the proposed method. The stiffness and mass of the intact model are the sum of the element matrices:

$$\mathbf{K} = \sum_{r=1}^{n_E} \mathbf{K}_r \tag{13}$$

$$\mathbf{M} = \sum_{r=1}^{n_E} \mathbf{M}_r \tag{14}$$

where $n_E$ is the number of elements, and $\mathbf{K}_r$ and $\mathbf{M}_r$ are respective contributions of the $r$th element to the global stiffness and mass matrices of the model. The reduction in the element stiffness and mass matrixes of the damaged structure determined from the intact model are

$$\delta\mathbf{K} = \sum_{r=1}^{n_E} \delta\mathbf{K}_r = \sum_{r=1}^{n_E} (\mathbf{K}_{rd} - \mathbf{K}_r) = \sum_{r=1}^{n_E} \delta k_r \mathbf{K}_r \tag{15}$$

$$\delta\mathbf{M} = \sum_{r=1}^{n_E} \delta\mathbf{M}_r = \sum_{r=1}^{n_E} (\mathbf{M}_{rd} - \mathbf{M}_r) = \sum_{r=1}^{n_E} \delta m_r \mathbf{M}_r \tag{16}$$

where $\delta k_r$ and $\delta m_r$ are scalar multipliers representing proportional changes in the stiffness and mass matrices of the $r$th element in the damaged state from their values in the intact state. Therefore, variations in the stiffness and mass matrices at the system level are expressed as the sum of changes in these matrices at the element level. For frame elements, (15) and (16) are decomposed to separately update various structural parameters (e.g., *EA*, *EI*, *GJ*, etc.).

Rewriting (9) using Eq. (12), after mathematical manipulations, the change of the dynamic response subjected to the applied harmonic load is obtained as

$$\delta\mathbf{X}(\omega) = S^S \delta\mathbf{k} + S^M \delta\mathbf{m} \tag{17}$$

$\mathbf{S}^S$ and $\mathbf{S}^M$ are analytical sensitivities of the dynamic response to the change in stiffness and mass parameters at the element level using a well approximated $\mathbf{H}_d(\omega)$. It is evaluated as

$$S^S_{(k,r)} = -\mathbf{H}^{-1}_{dk}(\omega)(\mathbf{K}_r)\mathbf{X}(\omega) \tag{18}$$

$$S^M_{(k,r)} = \mathbf{H}^{-1}_{dk}(\omega)(\omega^2\mathbf{M}_r)\mathbf{X}(\omega) \tag{19}$$

where $S^S_{(k,r)}$ is the $(k,r)$ entry of $\mathbf{S}^S$, stiffness-sensitivity matrix, and $S^M_{(k,r)}$ is the $(k,r)$ entry of $\mathbf{S}^M$, mass-sensitivity matrix. $\mathbf{H}_{dk}(\omega)$ is the $k$th row of the approximated transfer function of the damaged structures defined in (12), and $\mathbf{K}_r$ and $\mathbf{M}_r$ are the stiffness and mass matrices of the $r$th elements which are assembled into the global stiffness and mass matrices.

Changes in stiffness and mass properties can be determined using (17) by several methods such as the least square method (LS), non-negative least square method (NNLS), and singular value decomposition method (SVD). The quality of predicted damage by (17) depends on several factors including the sensor types and locations, excitation types and locations, the quality of measured FRF data (measurement error), selected frequency points for model updating, accuracy of the mathematical model (modeling error), observability of the unknown parameters, weighting techniques applied to the system of equations, and numerical methods used for solution of the system of equations. A balanced attention to these factors is expected to lead to less estimation errors in finite element model updating.

The least-squares solution is dominated by the equations with the largest numerical coefficients. This is caused by the types, locations and frequency ranges of excitation and the types and location of measurements. This means that some equations overshadow the information in other equations. Several methods have been suggested in the literature for weighting the system of equations. One may multiply both sides of each equation by a scaling factor so that the sum of square of coefficient in a resultant equation is unity, or omit some of the equations with smaller sensitivities to the unknown parameters [35,36]. If the $i$th equation associated with the frequency $\omega$ has elements $\mathbf{X}_i(\omega)$ and $\mathbf{X}_{id}(\omega)$ of similar magnitudes, the adverse effects of measurement errors may be significantly magnified after the weighting. To overcome

this problem, such an equation should be removed [35]. It is necessary to emphasize that deciding to remove such points in highly noise-contaminated regions is misleading and it is preferable to avoid such points of frequency for model updating.

In a more general form, the FRF of a structure can be evaluated using the velocity or acceleration responses, which are known as mobility and accelerance respectively:

$$\mathbf{V}(\omega) = \frac{\dot{\mathbf{X}}(\omega)}{\mathbf{F}(\omega)} = \omega \mathbf{H}(\omega) \tag{20}$$

$$\mathbf{A}(\omega) = \frac{\ddot{\mathbf{X}}(\omega)}{\mathbf{F}(\omega)} = -\omega^2 \mathbf{H}(\omega) \tag{21}$$

Comparison of (20) and (21) with (7) shows that the excitation frequency acts as a weighting factor on FRF data. If the identification process is carried out using a single excitation frequency data, there is no difference between results obtained by impedance, mobility and accelerance. In a multi-excitation frequency identification process, mobility and accelerance are weighted forms of the FRF of the structure by $\omega$ and $\omega^2$, therefore the solution of these equations might be dominated by the associated equation to the higher order of frequencies. Also, some researchers suggest multiplying each equation by $\omega^{-1}$ to decrease inaccuracy of the finite element modeling at higher frequency ranges [37]. In this paper, model updating is performed in selected frequency ranges. FRFs of the structure for each selected frequency point can be very different. Generally, equations related to the higher frequency have the lower amplitude and as a result will be overshadowed by the equation associated with lower frequencies. It should be noted that because of more localized behavior of structures at higher frequencies, these equations contain more information about damage. Therefore, in this paper, at individual mass and stiffness identification cases, each row of sensitivity equation matrix will be weighted by the inverse of its second norm. For simultaneous mass and stiffness parameters estimation no weight is applied. By this weighting, the contribution of the equation of higher frequency will be improved.

## 3. Application

The presented damage detection algorithm was applied to a six bay truss structure with the geometry and connectivity shown in Fig. 1. Each span is 2 m for a total of 12 m. The structure is modeled numerically using finite element method with basic structural elements, i.e. axial elements. Truss elements are made from steel with Young's modulus of 200 Gpa, mass density of 7300 of kg/m$^3$, and cross sectional areas are as given in Table 1. The degrees of freedom of this truss model are shown in Fig. 2.

The unknown parameters are axial rigidity of elements and $EA$ where $A$ is the cross-sectional area and $E$ is Young's modulus. Several damage scenarios are considered to investigate the influence of location, severity, and number of the damaged elements on the robustness of the proposed method. Table 2 shows specifications of these cases.

For the structure shown in Fig. 1, the FRF data should be either extracted from a non-destructive test or simulated numerically using the finite element method. Simulated data is used in this study. A single harmonic load is applied at the degree of freedom numbers 4, 8 and 17 at each load cases. Degrees of freedom numbers 1, 8, 14, 15, 20 and 21 are selected as six measurement locations. Measurement errors are considered by adding random errors to the simulated data from the finite element model. In this paper, 10 percent uniform random error has been added to the exact data of the finite element

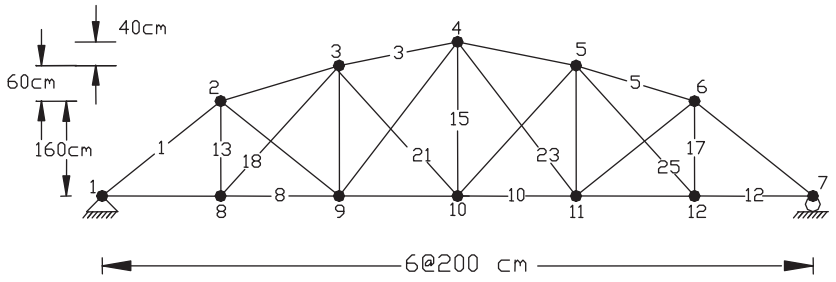


**Fig. 1.** Geometry of bowstring truss model.

**Table 1**
Cross-sectional area of truss members.

| Member | Area (cm$^2$) |
|---|---|
| 1–6 | 18 |
| 7–12 | 15 |
| 13–17 | 10 |
| 18–25 | 12 |

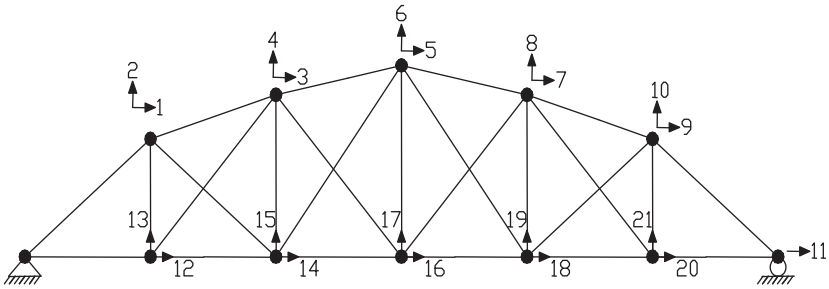


**Fig. 2.** Degrees of freedom of truss model.

**Table 2**
Percent of stiffness and/or mass reduction of truss elements.

| Case number | Element number and percent of damage | | | | | |
|---|---|---|---|---|---|---|
| 1 | Element no. | 7 | 18 | – | – | – |
| | Damage | 40% (K) | 50% (K) | – | – | – |
| 2 | Element no. | 7 | 14 | 18 | – | – |
| | Damage | 30% (K) | 30% (K) | 20% (K) | – | – |
| 3 | Element no. | 4 | 9 | 13 | 20 | 25 |
| | Damage | 20% (K) | 30% (K) | 30% (K) | 20% (K) | 20% (K) |
| 4 | Element no. | 6 | 14 | – | – | – |
| | Damage | 30% (M) | 25% (M) | – | – | – |
| 5 | Element no. | 10 | 18 | 25 | – | – |
| | Damage | 20% (M) | 20% (M) | 20% (M) | – | – |
| 6 | Element no. | 3 | 8 | 17 | 23 | – |
| | Damage | 30% (M) | 40% (M) | 40% (M) | 30% (M) | – |
| 7 | Element no. | 3 | 16 | 24 | – | – |
| | Damage | 30% (K) | 30% (K) | 30% (K) | – | – |
| | Element no. | 3 | 20 | – | – | – |
| | Damage | 30% (M) | 20% (M) | – | – | – |
| 8 | Element no. | 4 | 13 | 15 | 20 | 25 |
| | Damage | 30% (K) | 30% (K) | 30% (K) | 30% (K) | 30% (K) |
| | Element no. | 4 | 13 | 22 | – | – |
| | Damage | 30% (M) | 30% (M) | 20% (M) | – | – |

model. Some researchers assume that the natural frequencies of light damped structures can be measured noise-free or at least with a high level of confidence using available precise and low noise accelerometers and data acquisition systems [37].

The numerical simulation by the authors shows that adding 0.5 percent normally distributed random noise to the measured natural frequencies does not significantly impact the estimated parameters, if the excitation frequency of the applied loads are not in the vicinity of the nearest measured natural frequencies. Eq. (12) is used to illustrate this phenomenon. For undamped or light damped structures, the denominator of Eq. (12) and consequently $\mathbf{H}_d(\omega)$ is dominated by $\Omega_{id}^2 - \omega^2$. If the excitation frequency is selected close to the resonance frequency a small error in measured frequency introduces a significant change in $\Omega_{id}^2 - \omega^2$. By moving away from the resonance frequency this impact will be significantly reduced, resulting in a less measurement error-sensitive transfer function $\mathbf{H}_d(\omega)$. Additionally, by moving the excitation frequency away from resonance frequency, the response is less sensitive to damping and errors in damping measurements. Therefore, at all of the damage simulations in this study, noise-free natural frequencies have been considered and it has been assumed that the first 10 natural frequencies of the damaged structures are measurable at each load cases. The natural frequencies of the damaged structure are presented in Table 3.

Success of the proposed method is heavily dependent on the excitation frequency. Some practical rules for selecting this excitation frequency are given in [22]. The selected excitation frequency points must not be very close to the natural frequencies of the damaged structures to prevent resonance phenomena and noise-induced measurement. In addition, higher mode shapes are more local and therefore more sensitive to damage in comparison to lower mode shapes, although a large number of sensors must be provided to track their changes. Therefore, it is expected that higher excitation frequencies, which excite the higher mode shapes, yield better results.

Noting that the validation of $\delta\mathbf{X}(\omega)$ in (17) is dependent on the accuracy of $\mathbf{H}_d(\omega)$ in (12), proper adoption of excitation frequency becomes more important. $\mathbf{H}_d(\omega)$ is singular at the resonance frequencies. $\mathbf{H}_d(\omega)$ is insensitive to changes away from natural frequencies. Excitation frequencies should not be selected at resonance frequencies to avoid non-smooth and non-monotonous peaks of the transfer function. Since good sensitivities are achieved by approaching the natural frequencies [34], near resonance frequencies are recommended for measurements. Therefore, intermediate excitation frequencies ranges

**Table 3**
Natural frequencies of the damage cases.

| Mode no. | Intact | Damage case | | | | | | | |
|---|---|---|---|---|---|---|---|---|---|
| | | 1 | 2 | 3 | 4 | 5 | 6 | 7 | 8 |
| 1 | 30.3 | 29.2 | 29.6 | 29.3 | 30.6 | 30.8 | 31.3 | 30.4 | 30.4 |
| 2 | 69.0 | 63.0 | 65.1 | 67.2 | 69.8 | 70.0 | 70.6 | 68.6 | 68.6 |
| 3 | 96.3 | 96.3 | 96.2 | 95.6 | 97.5 | 97.8 | 99.4 | 96.1 | 96.5 |
| 4 | 181.8 | 172.4 | 176.5 | 176.4 | 183.6 | 183.7 | 187.9 | 180.0 | 181.7 |
| 5 | 223.2 | 220.8 | 221.7 | 214.7 | 227.8 | 226.3 | 229.1 | 221.5 | 209.7 |
| 6 | 275.6 | 268.2 | 271.4 | 267.4 | 279.0 | 279.0 | 284.2 | 275.4 | 271.9 |
| 7 | 321.6 | 320.3 | 309.5 | 319.4 | 323.9 | 324.5 | 334.5 | 303.7 | 303.6 |
| 8 | 352.0 | 338.0 | 335.1 | 340.6 | 355.0 | 357.0 | 358.1 | 343.8 | 342.0 |
| 9 | 357.7 | 355.4 | 349.7 | 349.8 | 360.8 | 361.8 | 365.6 | 354.5 | 355.9 |
| 10 | 373.0 | 368.3 | 369.0 | 363.7 | 375.7 | 378.0 | 386.7 | 372.4 | 368.9 |

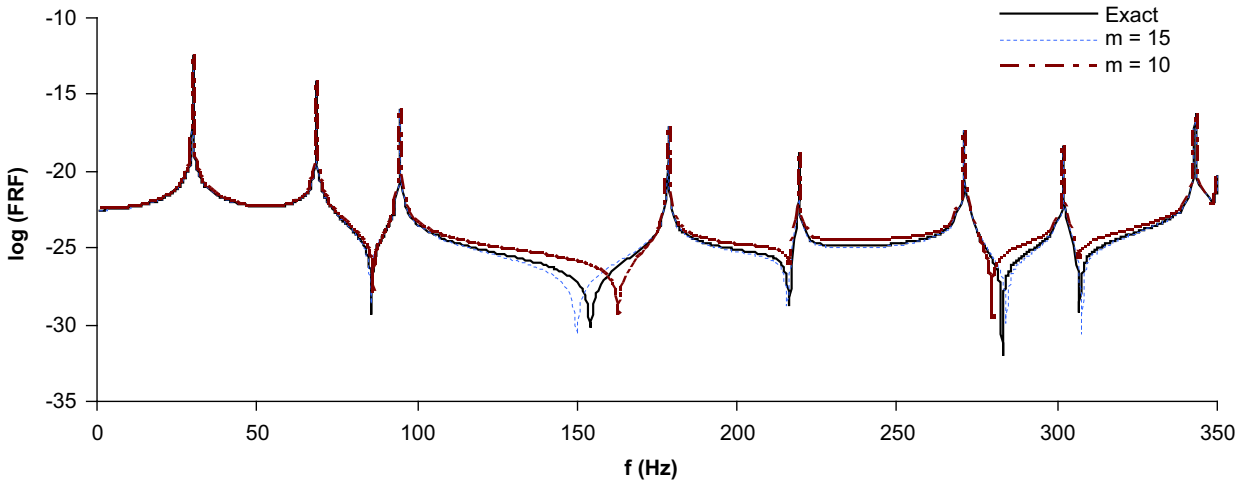


**Fig. 3.** Exact FRF of the damaged structure and approximate FRFs by Eq. (12).

are used for parameter estimations, (i.e., not in the immediate vicinity of resonances and not too far away from resonances). Also, the number of measured natural frequencies affects the accuracy of $\delta\mathbf{X}(\omega)$ in (17). Unmeasured natural frequencies affect the evaluated transfer function of the damaged structure $\mathbf{H}_d(\omega)$ and, consequently, the predicted parameters. For more illustration on the effects of incomplete frequency measurements and propagated errors in the transfer function of a typical FRF of a damaged structure, exact $\mathbf{H}_d(\omega)$ and its approximated evaluation by (12) are plotted in Fig. 3. These FRFs are related to the degree of freedom number 21 and subjected to the harmonic load at the degree of freedom number 10. Fig. 3 shows that Eq. (12) is more accurate at frequencies close to resonance frequencies. As mentioned before, the required number of measured natural frequencies to construct $\mathbf{H}_d(\omega)$ is dependent on the frequencies of excitation [38]. Fig. 3 indicates that for low excitation frequencies a good accuracy can be obtained using fewer measured natural frequencies, while for a higher range of excitation frequencies, more numbers of measured natural frequencies must be considered. Although Araujo dos Santos et al. [38] restrict the range of excitation frequencies based on the highest measured natural frequency for approximation of $\mathbf{H}(\omega)$, as shown in Fig. 3 the proposed formulation of approximate transfer function (12) is still valid in the high frequency range and close to resonances. This increases the chance of using higher excitation frequencies, even using a low number of measured natural frequencies for the damaged structure.

Using all of the FRF data for model updating is suggested by some researchers [33]; also excluding a part of the FRF data is recommended based on the previous discussions [34]. Using all of the data is not recommended by this study, since around the anti-resonance frequencies measurements are more noise contaminated. As stated before, $\mathbf{X}_i(\omega)$ and $\mathbf{X}_{id}(\omega)$ of similar magnitudes can adversely affect parameter estimation results and should be excluded from the range of frequencies used for model updating. Any decision for omitting such measured responses in the highly noise contaminated regions is misleading and it is preferred to avoid such regions in model updating. Hence, it is recommended that frequency points around anti resonances and far from resonances be excluded from model updating.

It should be mentioned that, in this method, the desired frequency range for model updating will be selected after measurement of the natural frequencies of the damaged structures. This way, one can select the frequency point of model updating at the region in which the occurred damage caused more changes in the natural frequencies, since the change of natural frequency consequently causes the change in the FRF.

Numerical simulation of this study shows that although for a low level of noisy data a few frequency points is enough for model updating, for higher levels of noise presence more data with a high sensitivity to the parameters changes can guarantee a robust parameters estimation. Therefore, in this paper a range of the frequency points close to analytical and corresponding measured resonances are considered for model updating except frequency points between them. The selected frequency ranges for model updating are given in Table 4 and used at 1 Hz intervals.

Monte Carlo simulations were conducted using different numbers of observations (i.e. 25, 50 and 100), and it was found that there is very little difference between the average of the estimated parameters and their standard deviation. Model updating processes at each Monte Carlo simulation did converge in 10–20 iterations. All of the reported results were obtained using 50 observations. Figs. 4–11 show results of the damage detection scenarios.

**Table 4**
Frequency ranges for model updating in each case.

| Damage case | 1 | 2 | 3 | 4 | 5 | 6 | 7 | 8 |
|---|---|---|---|---|---|---|---|---|
| Frequency ranges | 210–216 | 210–216 | 205–210 | 215–220 | 215–220 | 212–217 | 173–178 | 225–230 |
| | 227–235 | 227–235 | 228–235 | 230–240 | 230–240 | 233–240 | 183–188 | 260–268 |
| | 258–263 | 259–267 | 258–263 | 260–270 | 260–270 | 262–272 | 216–220 | 277–283 |
| | 278–285 | 279–285 | 278–285 | 283–290 | 283–290 | 290–299 | 224–227 | 295–300 |
| | 325–328 | 328–338 | 325–330 | 325–335 | 327–335 | 306–315 | 270–275 | 325–329 |
| | – | – | – | 363–368 | 364–369 | 390–400 | 277–280 | 330–339 |
| | – | – | – | – | 382–390 | – | 300–303 | 343–347 |
| | – | – | – | – | – | – | 335–343 | 359–364 |

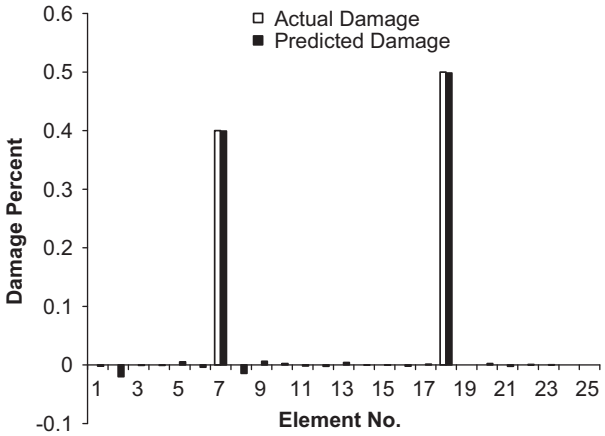


**Fig. 4.** Actual and predicted damage for case 1 (stiffness estimation).

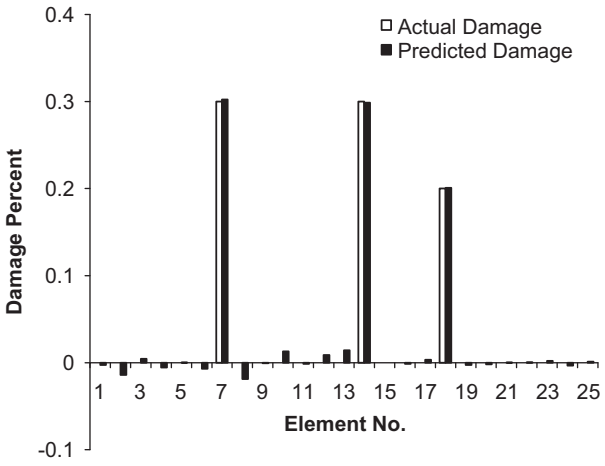


**Fig. 5.** Actual and predicted damage for case 2 (stiffness estimation).

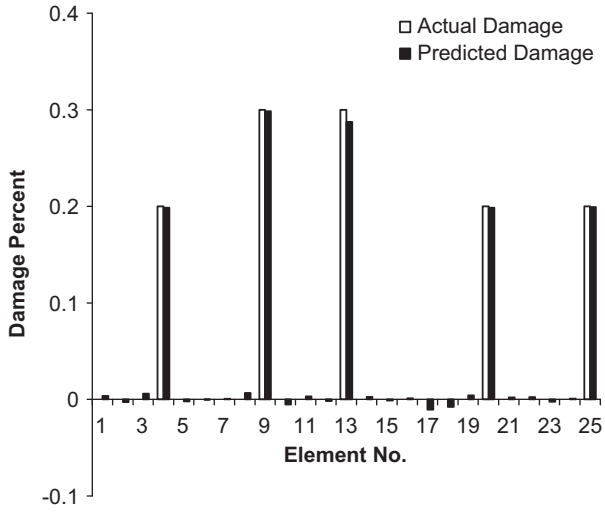


**Fig. 6.** Actual and predicted damage for case 3 (stiffness estimation).

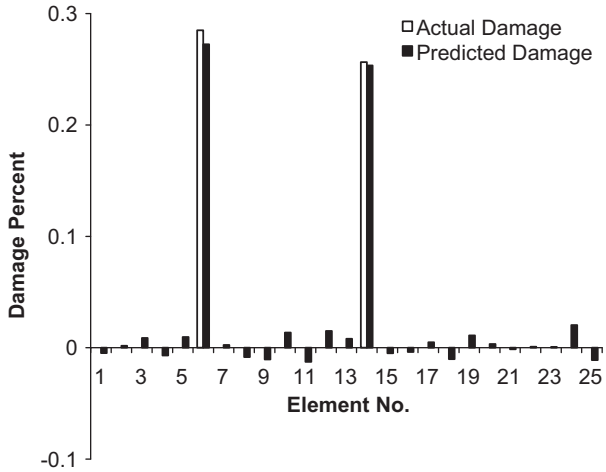


**Fig. 7.** Actual and predicted damage for case 4 (mass estimation).

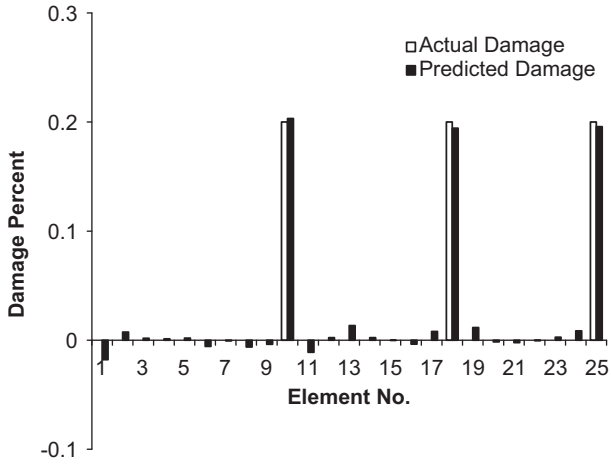


**Fig. 8.** Actual and predicted damage for case 5 (mass estimation).

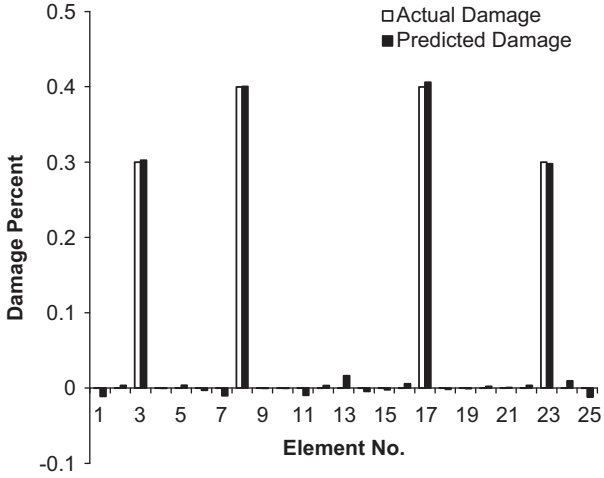


**Fig. 9.** Actual and predicted damage for case 6 (mass estimation).

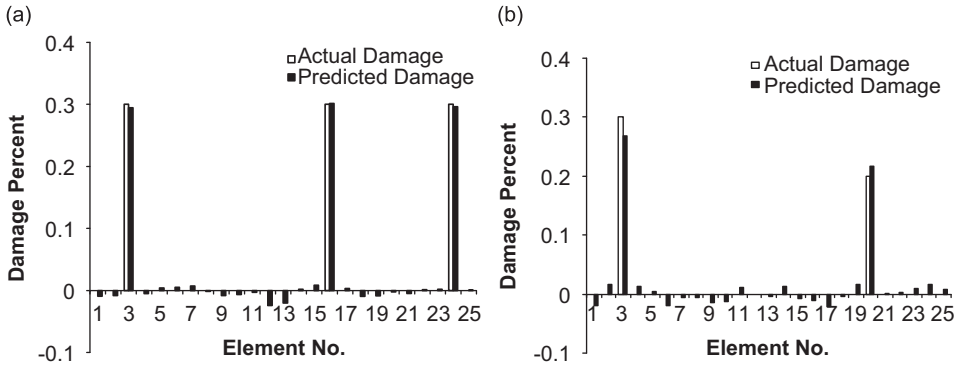


**Fig. 10.** Actual and predicted damage for case 7: (a) stiffness estimation; (b) mass estimation.

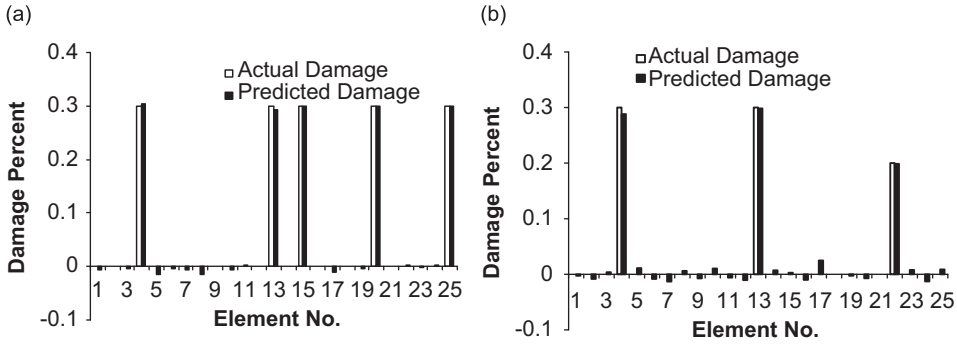


**Fig. 11.** Actual and predicted damage for case 8: (a) stiffness estimation; (b) mass estimation.

As illustrated by Figs. 4–11, this method is capable of detecting the damage location and severity using the incomplete noisy measured FRF data. In all damage cases, all 50 Monte Carlo simulations converged.

In stiffness updating processes, some deviation in stiffness identification is possible due to an inaccurate assumption regarding the mass of the intact and damaged structures. This inaccurate assumption introduces some errors in the undamaged eigenvector of the structures that will be used to construct sensitivity equations. In this study, numerical simulation proved that, at the selected excitation frequencies, considering 10 percent random error in mass matrices does not affect the results. It should be noted that for real structures in which the floor masses are more significant than the framing, mass modeling errors become more significant and it is necessity to consider mass model updating.

In structural dynamics, the mass matrix used in the FEM model is not an exact representation of the mass distribution effects, but the effect of using an incorrect mass on parameter estimation accuracy becomes low if a small excitation frequency is used. The reason is that the responses due to harmonic excitation are controlled by the transfer function described in Eq. (10), and $j\omega\mathbf{C}+\mathbf{K}$ becomes relatively large compared to $\omega^2\mathbf{M}$ with a small circular frequency. Therefore, the contribution of the mass matrix to the responses will be small, as is the contribution of inaccurate mass to the identification results.

The average of the estimated parameters does not reflect the robustness and confidence of the parameters estimation process. To investigate the robustness of a method, it is necessary to check the standard deviation of predicted unknown at Monte Carlo simulations. Low standard deviation indicates a robust method. For illustration purposes, standard deviation of the estimated parameters at the third case of damage scenarios is plotted in Fig. 12. Because this paper deals with the percentage of changes and not absolute values, presented standard deviations are unit-less.

Except of element number 8, Fig. 12 shows standard deviations of all predicted stiffness parameters of elements are low and indicate a robust solution. Also, the high standard deviation of element 8 indicates a low observability of this element compare to the other elements.

In order to quantify the accuracy and comparison of the predicted results, some indexes are used to evaluate the confidence level of the results. The damage missing error (DME) is defined as [39,40]

$$\mathrm{DME}=\frac{1}{N_T}\sum_{e=1}^{NT}\varepsilon_e^{\mathrm{I}} \quad \text{for } 0\le \mathrm{DME}\le 1 \tag{22}$$

where $N_T$ is the number of true damaged elements and $\varepsilon_e^{\mathrm{I}}=0$ if the location of truly damaged element is identified, or $\varepsilon_e^{\mathrm{I}}=1$ otherwise. If DME = 0, then all true locations of damaged elements are detected. False alarm error index is chosen as [39,40]

$$\mathrm{FAE}=\frac{1}{N_F}\sum_{e=1}^{N_F}\varepsilon_e^{\mathrm{II}} \quad \text{for } 0\le \mathrm{FAE}\le 1 \tag{23}$$

where $N_F$ is the number of the predicted damaged elements and $\varepsilon_e^{\mathrm{II}}=0$ if the predicted damaged element is truly damaged, or $\varepsilon_e^{\mathrm{II}}=1$ otherwise. If FAE = 0, then all predicted damaged elements are truly damaged elements. These damage indexes rely on the identification of the damage location and nothing is stated about damage severity.

Another index as mean sizing error [39] defines an average value of the absolute discrepancies between the true damage parameters $\delta\mathbf{P}_t$ and the predicted damage parameters $\delta\mathbf{P}_p$:

$$\mathrm{MSE}=\frac{1}{\mathrm{ne}}\sum_{e=1}^{n_E}|\delta\mathbf{P}_{te}-\delta\mathbf{P}_{pe}| \quad \text{for } 0\le \mathrm{MSE}\le\infty \tag{24}$$

Also the relative error

$$\mathrm{RE}=\frac{\sum_{e=1}^{ne}|\delta\mathbf{P}_{te}|-\sum_{e=1}^{ne}|\delta\mathbf{P}_{pe}|}{\sum_{e=1}^{ne}|\delta\mathbf{P}_{te}|} \quad \text{for } 0\le \mathrm{RE}\le 1 \tag{25}$$

and closeness index

$$\mathrm{CI}=1-\frac{\|\delta\mathbf{P}_t-\delta\mathbf{P}_p\|}{\|\delta\mathbf{P}_t\|} \quad \text{for } 0\le \mathrm{CI}\le 1 \tag{26}$$

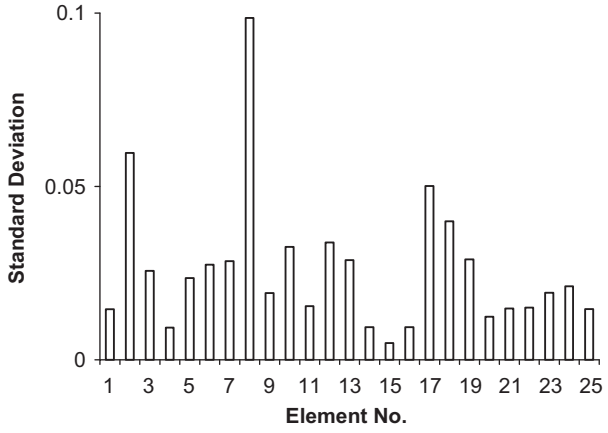


**Fig. 12.** Standard deviation of the estimated parameters for case 3.

**Table 5**
Comparison of damage indexes.

| Case no. | DME | FAE | DMS | RE | CI |
|---|---|---|---|---|---|
| 1 | 0 | 0 | 0.003 | −0.079 | 0.95 |
| 2 | 0 | 0.4 | 0.004 | −0.136 | 0.92 |
| 3 | 0 | 0 | 0.003 | −0.041 | 0.95 |
| 4 | 0 | 0 | 0.008 | −0.295 | 0.88 |
| 5 | 0 | 0.4 | 0.005 | −0.179 | 0.90 |
| 6 | 0 | 0.6 | 0.005 | −0.079 | 0.95 |
| 7 | 0 | 0.5 | 0.009 | −0.259 | 0.87 |
| 8 | 0 | 0.33 | 0.006 | −0.106 | 0.93 |

**Table 6**
Frequency ranges for mass deterioration case.

| | Set 1 | Set 2 | Set 3 | Set 4 |
|---|---|---|---|---|
| Frequency ranges | 205–212 | 170–176 | 233–240 | 210–215 |
| | 227–235 | 190–200 | 262–272 | 225–230 |
| | 250–258 | 212–217 | 290–299 | 265–270 |
| | 279–285 | 233–240 | 306–315 | 278–283 |
| | 300–312 | 262–272 | 390–400 | 304–310 |
| | 325–330 | 290–299 | – | 325–329 |
| | 363–366 | – | – | 365–368 |
| | 375–380 | – | – | 375–378 |

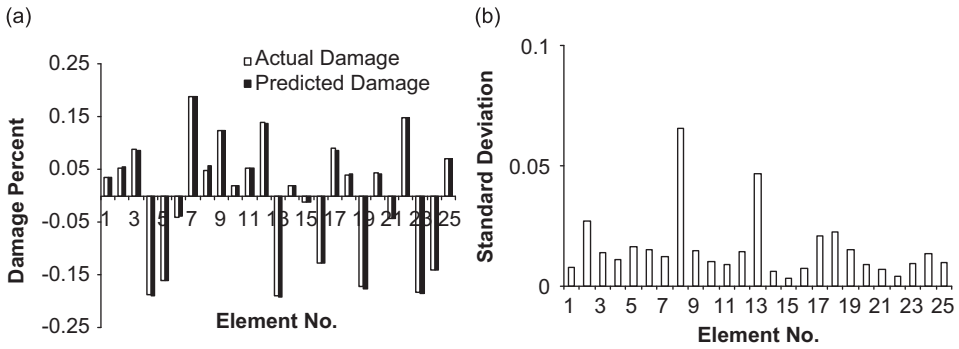


**Fig. 13.** Actual and predicted damage for the simulated deterioration in stiffness parameters: (a) stiffness estimation; (b) standard deviation.

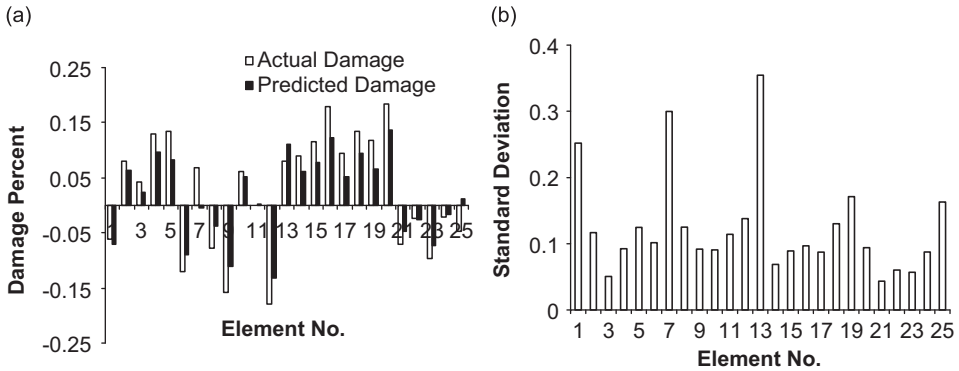


**Fig. 14.** Actual and predicted damage for the simulated deterioration in mass parameters: (a) mass estimation; (b) standard deviation.

are indexes of the distance between the true and computed damage parameters vectors. An element is taken as a damaged one if $|\delta k_p| \geq 2 \times \text{MSE}$ [39]. A comparison of the damage indexes of predicted results is given in Table 5. High levels of accuracy in parameter estimates are indicated by zero values of DME, FAE, DMS, RE and CI of 1.

As Figs. 4–11 and Table 5 show the proposed method is capable of localization of all damage elements. In addition to elements identified as truly damaged, some elements that appear so may not actually be damaged. This is due to the presence of noise in the FRF data, and sometimes to selected excitation frequency.

Damage is not always contained in a few elements, but might appear as deterioration of all structural elements in the case of corrosion. To investigate the applicability of the proposed method in such a case, stiffness parameters of all elements are contaminated with 20 percent random changes as a damage scenario Set 1 of frequency ranges in Table 6 is used for model updating. Fig. 13 shows the predicted damages and standard deviation of Monte Carlo simulations in this case.

Similar to the damage prediction case in Fig. 12, the maximum standard deviation in Fig. 14 is related to element number 8. In a similar case, 20 percent change of mass parameters resulted in the case being considered a damage case. Frequency ranges given by Set 2 in Table 6 are used for model updating. Predicted damage and its related standard deviation values are plotted in Fig. 14.

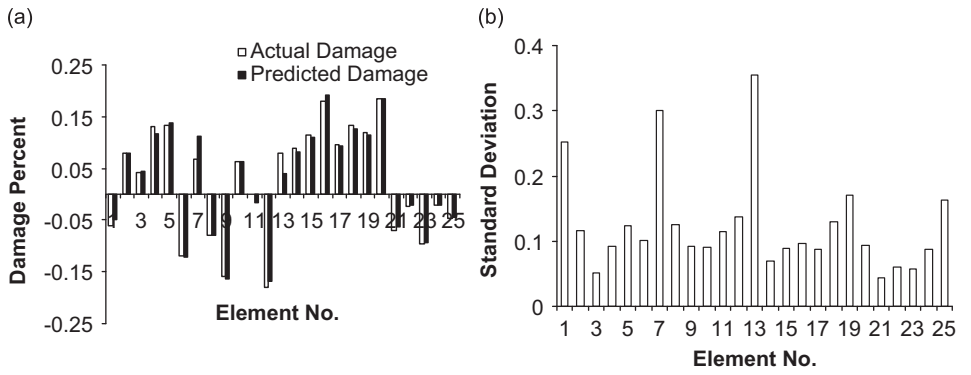


**Fig. 15.** Actual and predicted damage for the simulated deterioration in mass parameters by frequency set 3: (a) mass estimation; (b) standard deviation.

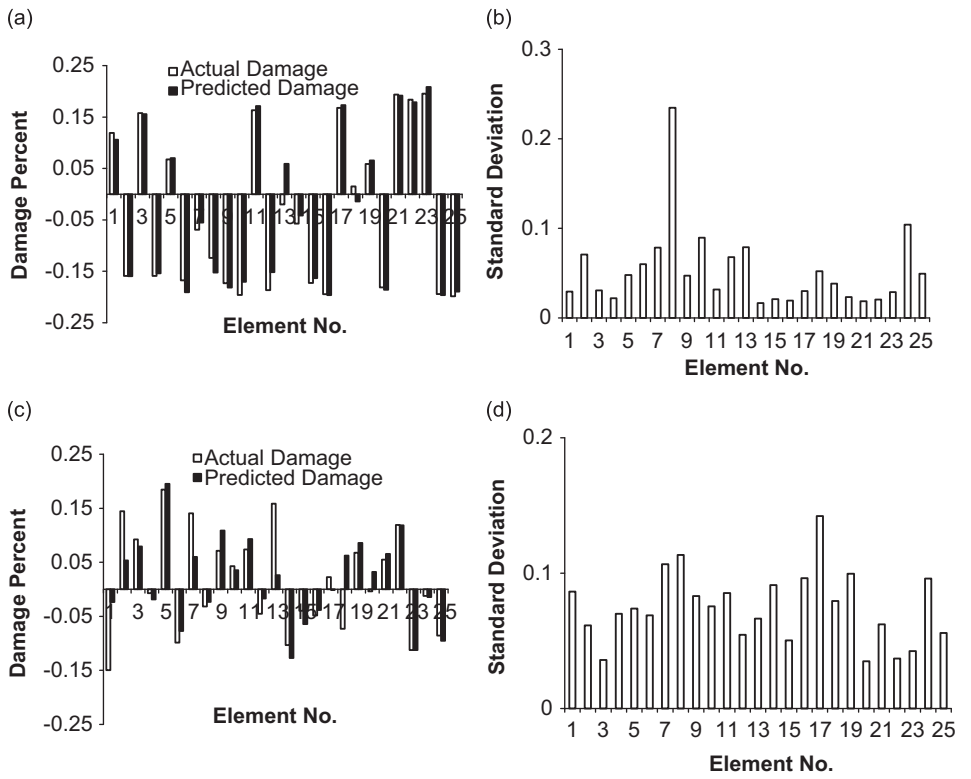


**Fig. 16.** Actual and predicted damage for the simulated deterioration in stiffness and mass parameters: (a) predicted stiffness parameters; (b) standard deviation of predicted stiffness parameters; (c) predicted mass parameters; (d) standard deviation of predicted mass parameters.

Fig. 14 shows less accuracy of the mass identification in comparison to the stiffness identification. As mentioned before, dynamic behavior at the lower frequencies is dominated by stiffness, and for better mass identification higher frequencies must be considered for model updating. In order to justify mass deterioration case was run using higher frequency ranges given by Set 3 of frequency ranges in Table 6, and results are plotted in Fig. 15.

Better parameter estimation and lower standard deviations proved that higher frequencies are better for mass estimations. It should be noted that this concept was tested in other cases, and the same results were found.

In a similar way deterioration in mass and stiffness parameters were considered simultaneously, and Set 4 in Table 6 is used for parameter estimation. Predicted parameters and their standard deviations are given in Fig. 16.

Fig. 16 indicates robust parameter estimations in the considered deterioration case in the mass and stiffness. As mentioned earlier, to have a more accurate evaluation of the transfer function of damaged structures $\mathbf{H}_d(\omega)$, an unmeasured part of modal characteristics of the damaged structures is replaced by the corresponding data of the intact structures (second term of (12)). To investigate the effects of omitting this part, it was excluded from (12) and damage case two was run again. Since the damage detection process has not been converged using 10 first frequency data, it became

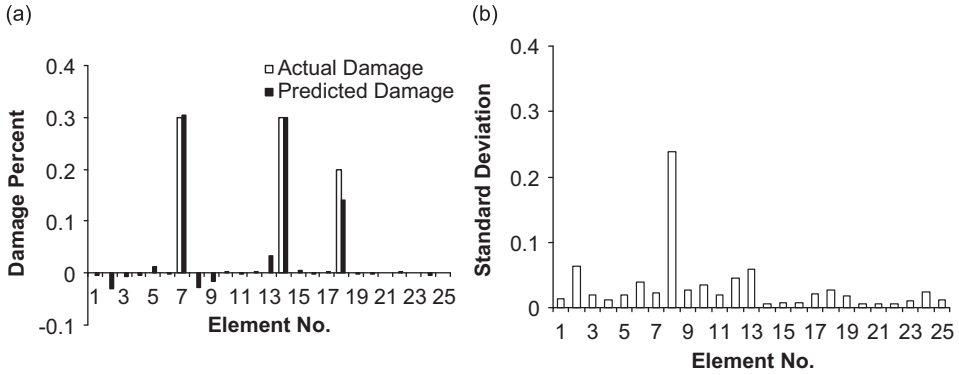


**Fig. 17.** Actual and predicted damage for case 3 without second part of $\mathbf{H}_d(\omega)$ in Eq. (12): (a) stiffness estimation; (b) standard deviation of the estimated stiffness parameters.

**Table 7**
Excitation frequency for each set.

| Frequency set | 1 | 2 | 3 | 4 |
|---|---|---|---|---|
| Frequency range | 55–63 | 85–90 | 165–172 | 205–210 |
| | 70–80 | 100–105 | 185–190 | 228–235 |
| | 85–90 | 165–172 | 205–210 | 258–263 |
| | 100–105 | 185–190 | 228–235 | 278–285 |
| | 165–172 | 205–210 | 258–263 | 310–315 |
| | 185–190 | 228–235 | 278–285 | 325–335 |

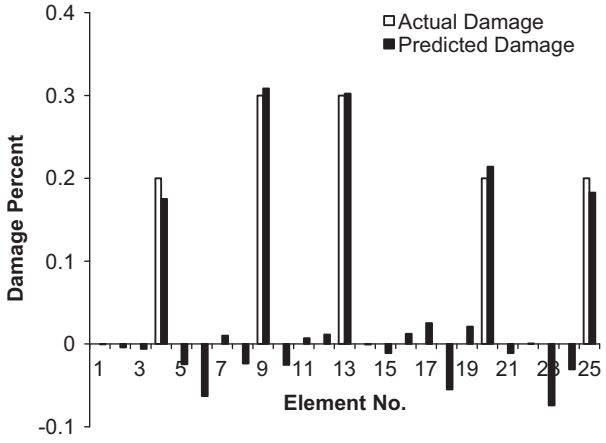


**Fig. 18.** Predicted damage by first frequency set for case 4.

necessary to include 16 first natural frequencies of the damaged structures, which is quite impractical. Also in this case 28 of 50 Monte Carlo simulations converged. Excluding the second term of (12) runs of most considered damage case show divergence of the solution using 10 first natural frequencies. Results of this case are given in Fig. 17.

To investigate the effect of the frequency of excitation on the accuracy of predicted results, in the fourth damage case the damage detection process has been done at several sets of frequency points. Excitation frequency ranges are given for each set in Table 7. Also in these runs 15 percent of uniform random noise is added proportionally to the simulated data.

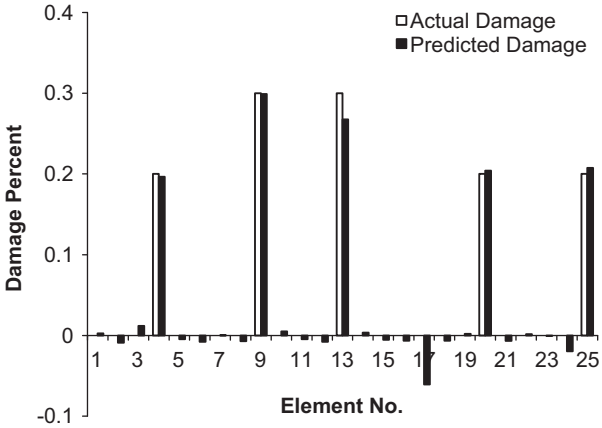


**Fig. 19.** Predicted damage by second frequency set for case 4.

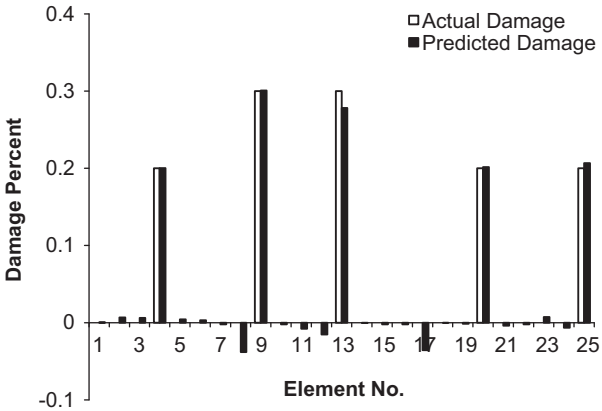


**Fig. 20.** Predicted damage by third frequency set for case 4.

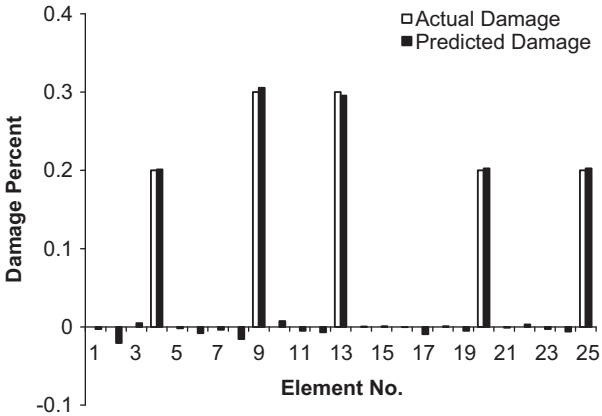


**Fig. 21.** Predicted damage by fourth frequency set for case 4.

**Table 8**
Damage index of frequency sets.

| Frequency set no. | DME | FAE | MSE | RE | CI | Number of converged observations |
|---|---|---|---|---|---|---|
| 1 | 0 | 0.375 | 0.019 | −0.33 | 0.75 | 41 |
| 2 | 0 | 0.251 | 0.010 | −0.12 | 0.85 | 49 |
| 3 | 0 | 0.285 | 0.007 | −0.11 | 0.89 | 50 |
| 4 | 0 | 0.285 | 0.005 | −0.09 | 0.94 | 50 |

Actual and predicted damage for the fourth case at different frequency sets are given in Figs. 18–21 and the associated damage index is given in Table 8.

As Table 8 shows, the best results are related to the fourth set, in which its excitation frequencies are selected at higher ranges. Also increasing CI and decreasing MSE and RE indicate higher accurate identification as frequency ranges go to higher ranges.

## 4. Conclusions

In this paper a structural damage detection method is presented using frequency response function and measured natural frequency. Elemental level sensitivity of the FRF of the structure to occurrence of damage is characterized as a function of changes of the stiffness and mass matrices, while effects of damping are included. Sensitivity equations are solved by least square method to achieve changes in structural parameters. Results of truss model show the ability of this method to identify location and severity of damages in the structural stiffness and mass. Effects of the excitation frequency on model updating were investigated and it was found that at most damaged cases, the best predictions are done using higher excitation frequencies.

## References

[1] R.D. Adams, P. Cawley, C.J. Pye, B.J. Stone, A vibration technique for non-destructively assessing the integrity of structures, *Journal of Mechanical Engineering Science* 20 (2) (1978) 93–100.
[2] H. Luo, S. Hanagud, An integral equation for changes in the structural dynamics characteristics of damaged structures, *International Journal of Solids and Structures* 34 (1997) 4557–4579.
[3] N. Bicanic, H.P. Chen, Damage identification in framed structures using natural frequencies, *International Journal of Numerical Methods in Engineering* 40 (1997) 4451–4468.
[4] S. Hassiotis, Identification of damage using natural frequencies and Markov parameters, *Computers & Structures* 74 (2000) 365–373.
[5] E.S. Bell, M. Sanayei, C.N. Javdekar, E. Slavsky, Multi response parameter estimation for finite-element model updating using nondestructive test data, *Journal of Structural Engineering* 133 (8) (2007) 1067–1079.
[6] Z. Wang, R.M. Lin, M.K. Lim, Structural damage detection using measured FRF data, *Computer Methods in Applied Mechanics and Engineering* 147 (1997) 187–197.
[7] S.K. Thyagarajan, M.J. Schulz, P.F. Pai, Detecting structural damage using frequency response functions, *Journal of Sound and Vibration* 210 (1) (1998) 162–170.
[8] P. Cornwell, S.W. Doebling, C.R. Farrar, Application of the strain energy damage detection method to plate-like structures, *Journal of Sound and Vibration* 224 (2) (1999) 359–374.
[9] J.S. Lew, Using transfer function parameter changes for damage detection of structures, *AIAA Journal* 33 (11) (1995) 2189–2193.
[10] A.K. Pandey, M. Biswas, Damage diagnosis of truss structures by estimation of flexibility change, *International Journal of Analytical and Experimental Modal Analysis* 10 (2) (1995) 104–117.
[11] J.M. Ricles, J.B. Kosmatka, Damage detection in elastic structures using vibratory residual forces and weighted sensitivity, *AIAA Journal* 30 (9) (1992) 2310–2316.
[12] P. Cawley, The impedance method of non-destructive inspection, *Journal of NDT International* 17 (1984) 59–65.
[13] H. Sohn, C.R. Farrar, F.M. Hemez, D.D. Shunk, D.W. Stinemates, B.R. Nadler, J.J. Czarnecki, *A Review of Structural Health Monitoring Literature: 1996–2001*, Los Alamos National Laboratory Report LA-13976-MS, 2004.
[14] S.W. Doebling, C.R. Farrar, M.B. Prime, D.W. Shevitz, Damage identification and health monitoring of structural and mechanical systems from changes in their vibration characteristics: a literature review, Los Alamos National Laboratory Report LA-13070-MS, April 1996.
[15] H.T. Banks, D.J. Inman, D.J. Leo, Y. Wang, An experimentally validated damage detection theory in mart structures, *Journal of Sound and Vibration* 191 (5) (1996) 859–880.
[16] J.S. Lew, Using transfer function parameter changes for damage detection of structures, *AIAA Journal* 33 (1995) 2189–2193.
[17] Z. Wang, R.M. Lin, M.K. Lim, Structural damage detection using measured FRF data, *Computer Methods in Applied Mechanics and Engineering* 147 (1997) 187–197.
[18] S.K. Thyagarajan, M.J. Schulz, P.F. Pai, J. Chung, Detecting structural damage using frequency response functions, *Journal of Sound and Vibration* 210 (1998) 162–170.
[19] R.P.C. Sampaio, N.M.M. Maia, J.M.M. Silva, Damage detection using the frequency–response–function curvature method, *Journal of Sound and Vibration* 226 (1999) 1029–1042.
[20] D.H. Lee, W.S. Hwang, Parametric optimization of complex systems using a multi-domain FRF-based sub structuring method, *Computers and Structures* 81 (2003) 2249–2257.
[21] F. Vestroni, D. Capecchi, Damage detection in beam structure based on frequency measurements, *Journal of Engineering Mechanics* 126 (7) (2000) 761–768.
[22] J.A. Pereira, W. Heylen, S. Lammens, P. Sas, Influence of the number of frequency points and resonance frequencies on model updating techniques for health condition monitoring and damage detection of flexible structure, *Proceedings of the 13th International Modal Analysis Conference*, Nashville, 1995, pp. 1273–1281.
[23] A.R. Choudhury, Damage Detection in Structures Using Measured Frequency Response Function Data, Ph.D. Thesis, Department of Mechanical Engineering, Victoria University of Technology, 1996.

[24] N.M.M. Maia, J.M.M. Silva, E.A.M. Almas, Damage detection in structures: from mode shapes to frequency response function methods, *Mechanical Systems and Signal Processing* 17 (3) (2003) 489–498.
[25] N.G. Park, Y.S. Park, Damage detection using spatially incomplete frequency response function, *Mechanical Systems and Signal Processing* 17 (3) (2003) 519–532.
[26] A. Furukawa, J. Kiyono, H. Iemura, Hi. Otsuka, Damage identification method using harmonic excitation force considering both modeling and measurement errors, *Earthquake Engineering and Structural Dynamic* 34 (2005) 1285–1304.
[27] U. Lee, J. Shin, A frequency response function-based structural damage identification method, *Computers and Structures* 80 (2002) 117–132.
[28] U. Lee, J. Shin, A structural damage identification method for plate structures, *Engineering Structures* 24 (2002) 1177–1188.
[29] U. Lee, K. Cho, J. Shin, Identification of orthotropic damages within a thin uniform plate, *International Journal of Solids and Structures* 40 (2003) 2195–2213.
[30] Y.Q. Ni, X.T. Zhou, J.M. Ko, Experimental investigation of seismic damage identification using PCA compressed frequency response functions neural networks, *Journal of Sound and Vibration* 290 (2006) 242–263.
[31] H.Y. Hwang, C. Kim, Damage detection in structures using a few frequency response measurements, *Journal of Sound and Vibration* 270 (1–2) (2004) 1–14.
[32] D.C. Zimmerman, T. Simmermacher, M. Kaouk, Model correlation and system health monitoring using frequency domain measurements, *Structural Health Monitoring* 4 (3) (2005) 213–227.
[33] J.V. Araujo dos Santos, C.M. Mota Soares, C.A. Mota Soares, N.M.M. Maia, Structural damage identification in laminated structures using FRF data, *Composite Structures* 67 (2005) 239–249.
[34] R. Pascuala, R. Schalchlib, M. Razetob, Robust parameter identification using forced responses, *Mechanical Systems and Signal Processing* 21 (2007) 1008–1025.
[35] Y. Ren, CF. Beards, Identification of joint properties of a structure using FRF data, *Journal of Sound and Vibration* 186 (4) (1995) 567–587.
[36] M. Sanayei, O. Onipede, Damage assessment of structures using static test data, *AIAA Journal* 29 (7) (1991) 1174–1179.
[37] K.S. Kwon, R.M. Lin, Robust finite element model updating using Taguchi method, *Journal of Sound and Vibration* 280 (2005) 77–99.
[38] W.X. Ren, G. De Roeck, Structural damage identification using modal data I: simulation verification, *Journal of Structural Engineering* 128 (2001) 87–95.
[39] J.T. Kim, N. Stubbs, Model-uncertainty impact and damage detection accuracy in plate girder, *Journal of Structural Engineering* 121 (10) (1995) 1409–1417.
[40] C.-B. Yun, J.-H. Yi, EY. Bahng, Joint damage assessment of framed structures using a neural networks technique, *Engineering Structures* 23 (2001) 425–435.